ACS Photonics

Article

pubs.acs.org/journal/apchd5

High-*Q* Microcavity Enhanced Optical Properties of $CuInS_2$/ZnS Colloidal Quantum Dots toward Non-Photodegradation

Yue Sun,[†] Feilong Song,[†] Chenjiang Qian,[†] Kai Peng,[†] Sibai Sun,[†] Yanhui Zhao,[†] Zelong Bai,[‡] Jing Tang,[†] Shiyao Wu,[†] Hassan Ali,[†] Fang Bo,[§] Haizheng Zhong,[‡] Kuijuan Jin,[†,⊥,∥] and Xiulai Xu*[,†,⊥]

[†]Beijing National Laboratory for Condensed Matter Physics, Institute of Physics, Chinese Academy of Sciences, Beijing 100190, China

[‡]Beijing Key Laboratory of Nanophotonics and Ultrafine Optoelectronic Systems, School of Materials Science & Engineering, Beijing Institute of Technology, Beijing 100081, China

[§]The MOE Key Laboratory of Weak Light Nonlinear Photonics, TEDA Applied Physics Institute and School of Physics, Nankai University, Tianjin 300457, China

[⊥]School of Physical Sciences, University of Chinese Academy of Sciences, Beijing 100190, China

[∥]Collaborative Innovation Center of Quantum Matter, Beijing, China

ABSTRACT: We report on a temporal evolution of photoluminescence (PL) spectroscopy of $CuInS_2$/ZnS colloidal quantum dots (QDs) by drop-casting on SiO_2/Si substrates and high quality factor microdisks (MDs) under different atmospheric conditions. Fast PL decay, peak blue shift, and line width broadening due to photooxidation have been observed at low excitation power. With further increasing of the excitation power, the PL peak position shows a red shift and the line width becomes narrow, which is ascribed to the enhanced Förster resonant energy transfer between different QDs by photoinduced agglomeration. The oxygen plays an important role in optically induced PL decay, which is verified by a reduced photobleaching effect under vacuum. When the QDs are drop-casted on MDs, photooxidation and photobleaching are accelerated because the excitation efficiency is greatly enhanced with coupling the pumping laser with the cavity modes. However, when the emitted photons couple with cavity modes, a PL enhancement by more than 20 times is achieved because of the increased extraction efficiency and Purcell effects of MDs at room temperature (RT) and 35 times at 20 K. The photobleaching can be avoided with a small excitation power but with a strong PL intensity by taking advantage of high quality factor cavities. The highly efficient PL emission without photodegradation is very promising for using $CuInS_2$ QDs as highly efficient photon emitters at RT, where the photodegradation has always limited the practical applications of colloidal quantum dots.

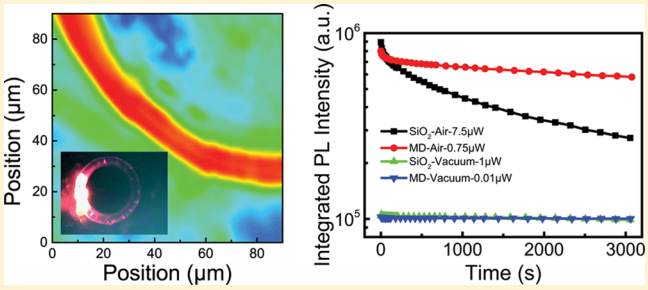

KEYWORDS: *$CuInS_2$, colloidal quantum dots, high quality factor, microcavity, photodegradation*

Compared to the traditional II–VI colloidal quantum dots (QDs),[1−5] copper indium sulfide (CIS) QDs,[6−9] also called nanocrystals, have been investigated intensively as an alternative for having less toxic materials such as cadmium or lead. Because of the large Stokes shift of about 300 meV[10] and the wide emission energy tunability,[6] CIS QDs have been explored in many applications such as light-emitting diodes,[6] photovoltaics,[11] and bioimaging.[12] CIS QD-based light-emitting diodes have been demonstrated with a high electroluminescence intensity and a spectrum range from the visible to near-infrared region.[6,13] Recently, a high photoluminescence (PL) quantum yield up to 86% has been demonstrated in core/shell structured QDs.[14] Up to now, the radiative decay mechanism of CIS QDs is not very well understood,[13,15−17] which could be the recombination from a conduction band to localized intragap state,[14,17,18] from a donor−acceptor pair (DAP),[19,20] or from a localized state to valence band.[21] In addition, instability of fluorescence always limits the colloidal QDs from commercialization because of the photooxidation and photobleaching, which has been studied mainly in conventional II–VI QDs.[4,5,22] However, photodegradation of CIS QDs has rarely been investigated so far.[16,23] Therefore, understanding the photoinduced degradation mechanism of CIS QDs systematically is highly desirable for a practical utilization of colloidal QDs.

Optical microcavities have been used to implement light–matter interactions because of the strong light confinement,[24,25] such as investigating cavity quantum electrodynamics and obtaining the emitted photons in desired directions. When the colloidal QDs are coupling with microcavities, enhanced photon emission from colloidal QDs has been observed with

Received: November 1, 2016
Published: January 12, 2017

DOI: 10.1021/acsphotonics.6b00843
ACS Photonics 2017, 4, 369−377

optical cavities[26−34] and plasmonic cavities[35,36] by greatly suppressing the spontaneous emission lifetime. Strong coupling between an exciton in a QD and a photon in a high quality factor (Q) optical resonator has been reported recently[37−41] when the exciton energy is resonant with the cavity mode. Among these microcavities, microdisks (MD) are relatively easy to fabricate and have a very high Q of whispering-gallery modes (WGMs).[40,42,43] Due to the large size of the MDs, they provide a great opportunity to drop-cast QDs on MDs for investigating the enhancement of optical properties of colloidal QDs.

To couple the colloidal QDs with the MDs, QDs have been embedded inside the MD cavity to maximize the coupling strength due to the better field overlapping.[28,43] However, this makes the fabrication processes of MDs much more complex and also limits the Q because of the nonuniformity of the QD layer. In fact, the QDs could couple efficiently the evanescent electric field of cavity modes when QDs are drop-casted on top of the cavities, which also enhances the optical properties of QDs.[32,33] In this work, we report on the temporal evolution of the PL properties of colloidal CIS/ZnS QDs dispersed on SiO_2/Si substrates and MDs. The PL intensity of QDs on the edge of MDs is greatly enhanced by 20 times at room temperature (RT) and 35 times at 20 K because of the Purcell effect of MDs. It is found that the PL intensity of close-packed CIS/ZnS QDs initially decreases and then remains stable with CW laser illumination, which can be ascribed to photobleaching and photooxidation. The photoinduced degradation is investigated under air and vacuum atmospheric environments at different temperatures. We found that optically induced degradation can be avoided with a small excitation power by taking advantage of enhanced PL emission using MDs.

RESULTS AND DISCUSSION

Figure 1 shows a schematic diagram of a conventional confocal micro-PL system for PL measurement of QDs on SiO_2/Si substrates and MDs (as shown in the inset). Figure 2a−c show wide-field PL images of CIS QDs on a MD by shining a pumping laser at different locations. During the PL mapping, the pumping laser was filtered out with a long-pass filter. When the pumping laser touches the edge of the MD, as shown in Figure 2a, the contacting part turns red due to the PL, while the opposite MD edge away from the laser spot remains dark. When the laser totally irradiates on the edge of a MD, the whole edge of the MD turns on, which is demonstrated in Figure 2b. This indicates that the pumping laser couples to the WGMs of the MD, which excites the QDs on the edge. Another possibility is that the emitted light from QDs also couples to the cavity modes. After the laser goes far away from the edge of the MD, the PL intensity becomes weak, as shown in Figure 2c. To illustrate the cavity modes of the MD, a two-dimensional finite-difference time-domain method was used to simulate the cavity modes. Figure 2d shows electric field magnitude distribution of a TE mode of about 669.75 nm, which is close to the center of the PL spectrum. The enlarged cavity mode distribution is shown in the inset of Figure 2d. It can be seen that the simulated field distribution on the edge of the MD corresponds well with the observed PL images.

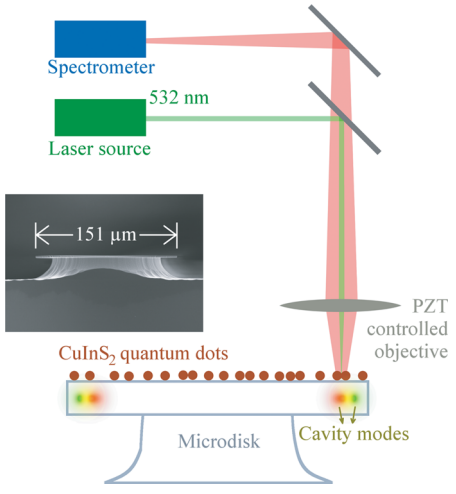

Figure 1. Schematic diagram of a confocal micro-PL system for QDs on MDs. The objective lens is mounted on a two-dimensional PZT-controlled stage for PL mapping. A scanning electron microscopy image of cross section of a typical MD is shown in the inset.

To get detailed spectral information, the PL spectra were mapped by moving the objective in a step of 1.5 μm. Figure 3a and c show the PL mapping of the QDs of a quarter of an area of the MD at RT and 20 K. The red annulus similar to the edge of the MD shows an enhancement of the PL, which is induced by the cavity modes of the MD. The PL spectra from the edge of the MD and from outside the MD are shown in Figure 3b and d. The integrated PL intensity on the edge of the MD (black dashed line) is enhanced by 20 times compared with that of the QDs outside the MD (red solid line) at RT, and an enhancement of 35 times was observed at 20 K. In general, MDs with a large diameter of around 150 μm have a high density of WGMs and the mode separations are very small (less than 0.1 nm). Such a small mode separation is less than our spectrometer resolution of about 0.1 nm. Therefore, we cannot resolve the different modes of the MD as before.[43] Normally, the cavity modes in different wavelengths could have different quality factors, which results in a different enhancement in the PL spectrum range of the QDs. However, the inset of Figure 3b shows the normalized PL spectra of different positions, which are in the exact same line shape. This verifies that the cavity enhances the PL emission with the same degree for the emission wavelength range of CIS QDs.

As a comparison, SiO_2/Si wafers have been used as substrates to drop-cast QDs for optical spectroscopy measurement. Figure 4a and b describe the temporal evolution of PL spectra of close-packed CIS/ZnS QD solids on a SiO_2/Si substrate with an excitation power of about 300 μW in air and under vacuum, respectively. The PL spectra are clearly affected by the laser irradiation time and the environment. In air, the PL intensity initially decreases rapidly and then gradually stabilizes, as shown in Figure 4a. The overall PL intensity reduces to around 10% with an irradiation time of 3000 s. It is well known that the decreasing PL intensity of colloidal QDs is due to the photooxidation and the photobleaching.[4,44] To separate photooxidation and photobleaching effects, a similar PL measurement was performed under vacuum as shown in Figure 4b. It can be seen that the PL intensity decreases in a slower manner compared with that in air. Without considering the photooxidation, the PL decay as a function of time is due to the photobleaching. The photobleaching can be explained by the fact that optically induced damage of oleylamine (OLA) introduces defect states at the surface of CIS/ZnS QDs, resulting in nonradiative channels in the recombination.

To further show the photooxidation-induced PL decay behavior, the time evolution of normalized PL intensity with

DOI: 10.1021/acsphotonics.6b00843
ACS Photonics 2017, 4, 369−377

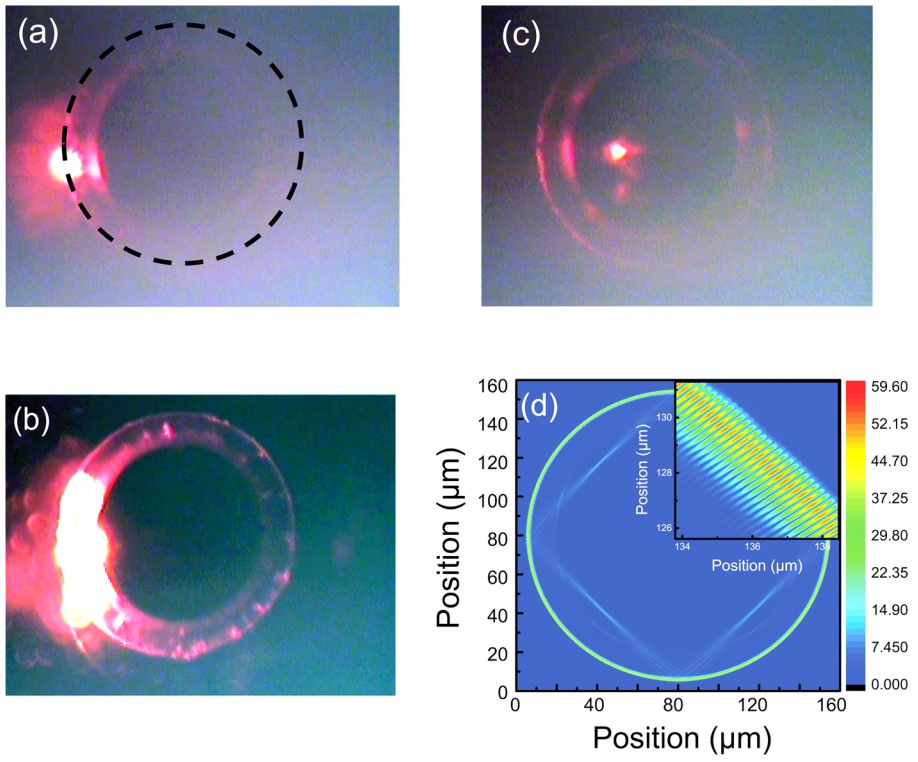

Figure 2. Wide-field PL images of CIS QDs on a MD by moving the pumping laser spot crossing the edge of the MD close to the edge (a), on the edge (b), and away from the edge (c). The pumping laser was filtered when the images were captured. (d) Magnitude of the electric field distribution of a cavity mode at 669.75 nm of the MD, which was simulated by a finite-difference time-domain method with the following parameters: r = 75 μm, n_{SiO_2} = 1.456, mesh = 25 nm. The inset shows an enlarged pattern of the mode distribution.

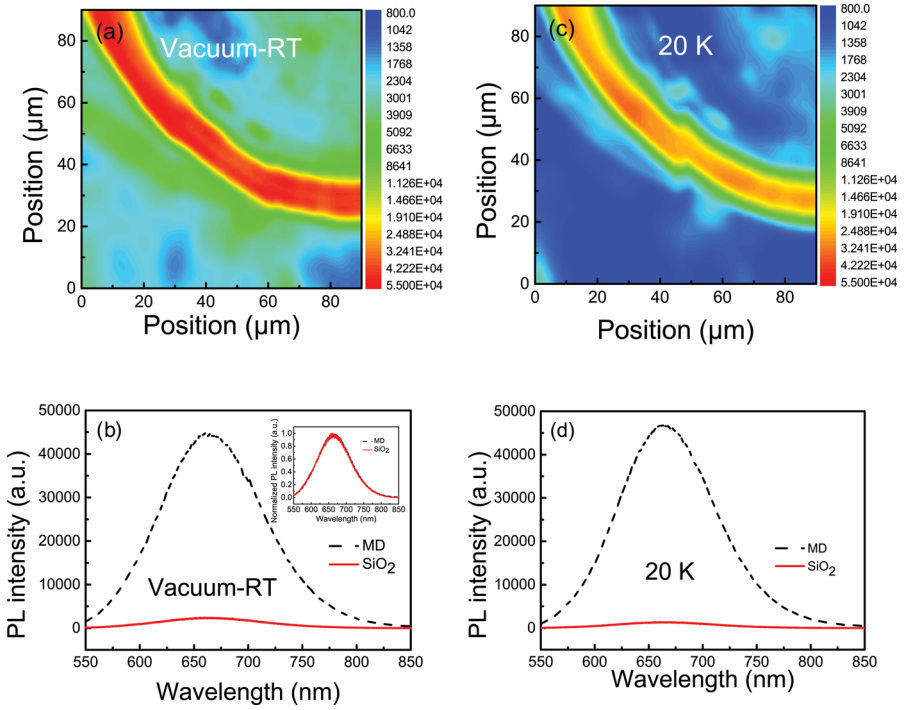

Figure 3. (a and c) PL mapping of CIS/ZnS QDs on MDs with a scanning area of 80 × 80 μm^2. The color bars are in log scale. (b and d) Typical PL spectra of close-packed CIS QD solids at RT and at 20 K. The black dashed lines are the PL spectra of QDs on the edge of the MD, and the red solid lines are PL spectra collected far away from the MD. The inset in (b) shows the normalized PL spectra of QDs.

different excitation powers under air and vacuum is shown in Figure 4c and d, respectively. In general, the higher the excitation power, the faster the decay of the PL intensity both in air and under vacuum. For the sample exposed in air, the PL decay rate increases with increasing the excitation power up to 120 μW and then saturates, but the decay rate in the vacuum

DOI: 10.1021/acsphotonics.6b00843
ACS Photonics 2017, 4, 369−377

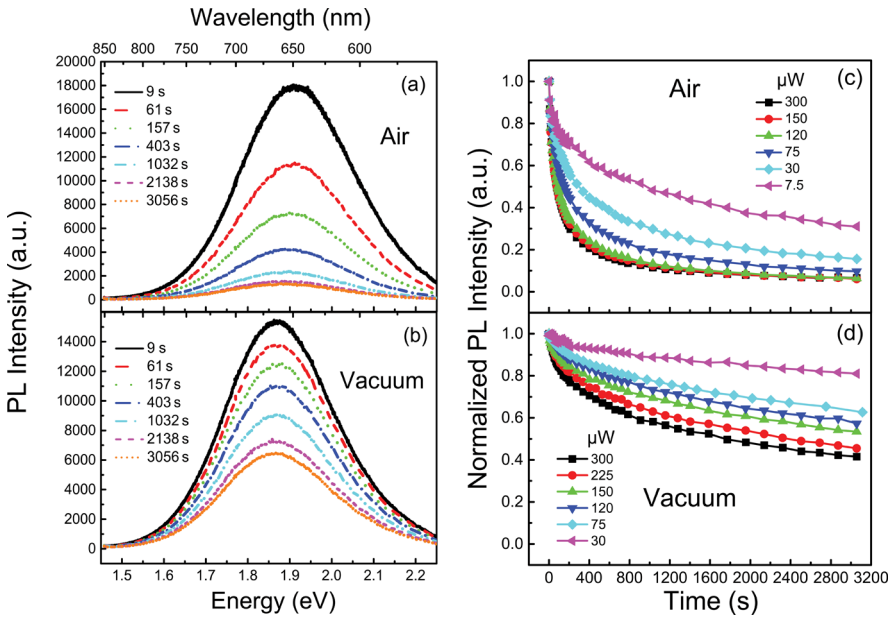

Figure 4. PL spectra of the close-packed CIS/ZnS QDs on SiO_2/Si substrates as a function of irradiation time in air (a) and under vacuum (b). (c and d) Normalized PL intensity decay as a function of time for the CIS/ZnS QDs on SiO_2/Si substrates under different excitation power in air and under vacuum.

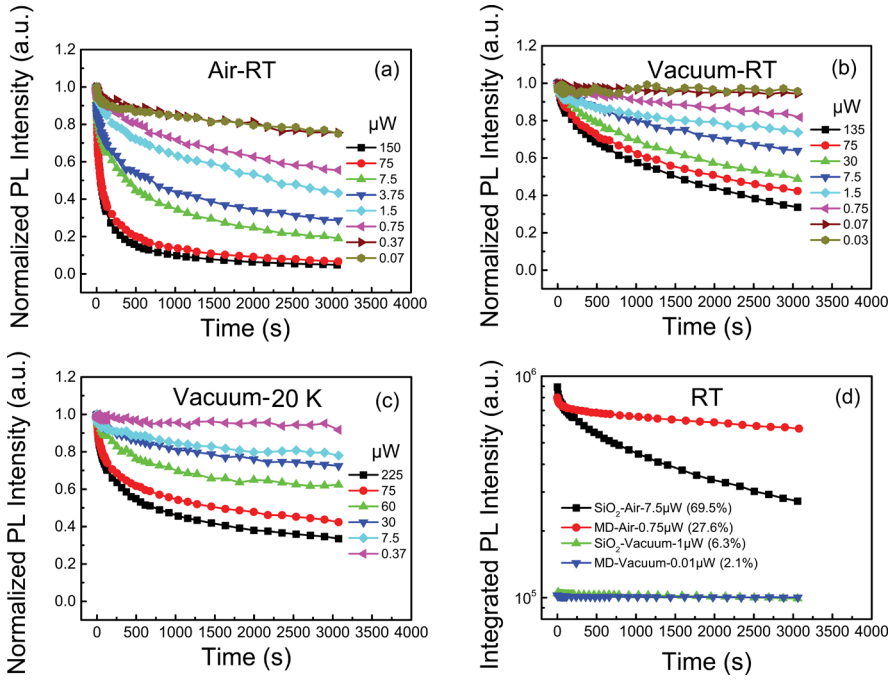

Figure 5. Normalized PL decay as a function of time for CIS/ZnS QDs on the edge of MDs under different excitation power in air (a), under vacuum (b) at RT, and at a low temperature of 20 K (c). (d) Comparison of the temporal evolution of integrated PL intensities for QDs on SiO_2/Si substrates and MDs. The excitation power for each substrate was tuned to achieve similar PL intensities in air and under vacuum. The PL intensity decay percentage for each line is labeled in the figure legend.

increases monotonically. At a fixed value of excitation power, the PL intensity in air decreases faster than that under vacuum, as discussed above. For example, at an excitation power of 300 μW, the PL intensity drops more than 80% in the first 400 s and continues to drop with a slower rate within the rest of the measuring time. While under vacuum, the PL intensity decreases by around 30% after 400 s, and no clear saturation can be observed within the measurement time of about 3000 s.

Similarly, time-dependent PL measurement has been performed on the edge of MDs where the PL emission is greatly enhanced, as shown in Figure 5, at different atmospheric environments (air or vacuum) and different temperatures (RT or 20 K). Comparing with Figure 4c for QDs exposed in air, a similar PL decay is observed at high excitation power. For instance, the PL intensity under an excitation power of 150 μW drops to 80% after exposure of about 200 s in air and then stabilizes. In vacuum or under low temperature as shown in

DOI: 10.1021/acsphotonics.6b00843
ACS Photonics 2017, 4, 369−377

Figure 5b and c, the behavior of the PL decay is similar to the case when QDs are on the SiO_2/Si substrate under vacuum (Figure 4d). The higher the excitation power, the faster the decay of the PL, which further confirms the photobleaching process. It should be noticed that with low excitation power the photobleaching effect becomes negligible, for instance, 0.03 μW under vacuum at RT and 0.37 μW at low temperature as shown by the top traces in Figure 5b and c, respectively.

To understand the cavity-enhanced emission for CIS/ZnS QDs on an MD, we first consider that QDs on MDs are coupling with the modes of the cavity, which enhances the extraction PL efficiency of QDs.[33] Since the MDs in this work have a large diameter, the cavity modes cover a broad wavelength range including both the emission wavelength range of QDs from 550 to 850 nm and the excitation wavelength at 532 nm. When the excitation laser illuminates with a high excitation power on the edge of the MD with a laser spot of 1−2 μm in diameter, photoluminescence can be observed from the QDs on the edge of the whole MD, as shown in Figure 2a. This confirms that the pumping laser couples to the modes in the cavity and circulating in the cavity, which excites all the QDs on the edge of the MD. Additionally, the emitted photons from QDs under the illumining spot coupling with the WGMs of the MD are extracted more efficiently, resulting in an enhanced emission.

Another reason for the enhanced emission is the Purcell effect, where the QDs couple with the cavity modes in a weakly coupling regime.[29] In this case, the spontaneous emission rate is enhanced by suppressing the luminescence lifetime of the QDs, which enhances the PL emission. Here, no clear increase was observed in the slope of the emission intensity versus the excitation intensity, which is due to the amplified spontaneous emission. This might be caused by the enhancement of photooxidation, photobleaching, and the Auger effect with increasing pumping power.[9] With a reduced lifetime of the QDs, the fast Auger process (around 100 ps) could also be suppressed, resulting in an increased biexciton emission in the QDs.[45] This needs to be confirmed with further measurement using ultrafast time-resolved PL measurement. Nevertheless, excitation power can be greatly reduced to achieve the same emission intensity with QDs on the edge of MDs, compared with that on SiO_2/Si substrates. The excitation power can be reduced from 7.5 μW to 0.75 μW to achieve a luminescence intensity of 1 million counts/s with QDs on the MDs, as shown in Figure 5d. It can be seen that the rates of the photooxidation and photobleaching are greatly reduced because of the smaller excitation power in the vacuum at RT. One striking observation is that photoinduced degradation almost disappears with a small excitation power, while a relatively high emission intensity is obtained with an excitation power of 0.01 μW on MDs under vacuum at RT. The integrated PL intensity decreased only by 2.1% within the measurement time, as shown by inverted blue triangles in Figure 5d, which still can be improved. But for QDs on SiO_2/Si substrates, an optically induced PL intensity decrease by 6.3% is observed for similar PL intensity since it requires a pumping power of 1 μW (green triangles in Figure 5d). No PL degradation under vacuum makes CIS/ZnS QDs very promising for highly efficient photon emission for quantum information processing.[46−49]

The PL decay of CIS/ZnS QDs can be fitted by a biexponential form as $A_1 \exp(-t/\tau_1) + A_2 \exp(-t/\tau_2)$.[50] Two time constants, τ_1 and τ_2, can be extracted by the fitting PL decay in Figures 4 and 5. Figure 6 summarizes the time

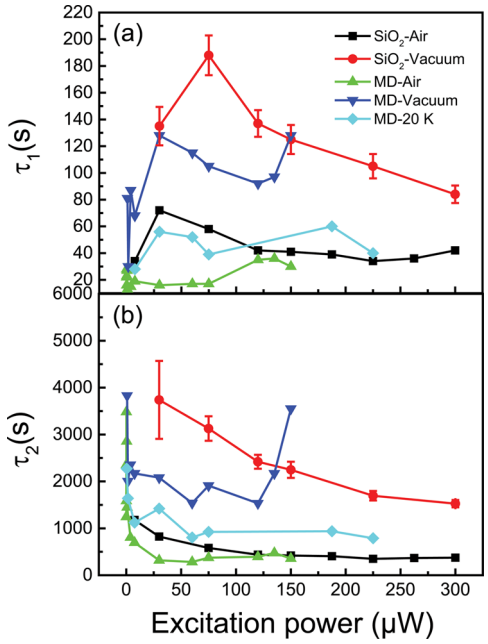

Figure 6. Fitted time constants τ_1 (a) and τ_2 (b) of PL decay as a function of excitation power for QDs on SiO_2/Si substrates and MDs in air or under vacuum at RT or at 20 K. The error bars are marked only for QDs on a SiO_2/Si substrate under vacuum to avoid complexity.

constants of the decay of integrated PL intensity as a function of excitation power with continuous irradiation. The fast decay constant τ_1 is in the range of 10 to 160 s, but τ_2 varies in the range of 300 to 3700 s. At RT, both τ_1 and τ_2 in air are much smaller than those under vacuum, which means that oxygen in the air induces mainly the photooxidation and photobleaching as reported before.[4] As mentioned before, the PL decays faster with increasing the excitation power. Here, the required excitation power on the MDs is much smaller than that on SiO_2/Si substrates, where it has similar decay rates. This is due to the fact that the pumping laser is coupled to the cavity modes, which enhances the excitation efficiency and accelerates the photooxidation process in CIS QDs. It should be noticed by contrast that photoinduced degradation is surprisingly small with a low excitation power, which gives a very long decay time constant τ_2. The time constants of PL decay of the sample at 20 K are much smaller than those under vacuum at RT, but are larger than those in air. This could be due to the fact that the OLA ligands are more easily damaged by the laser at low temperature, resulting in a faster PL decay.

Under a continuous illumination with a pumping laser, temporal evolution of the peak position and line width of PL spectra is very useful to understand the mechanism of photoinduced degradation.[4,5] The variations of PL peak position and the full width at half-maximum (fwhm) as a function of irradiation time are depicted in Figure 7 and Figure 8, respectively. Figure 7a represents the PL peak shifting of QDs on the edge of an MD under different excitation power in air. Since the photodegradation here is an irreversible process for QDs, the laser spot was moved to different places for each measurement when the excitation power was changed. It can be seen that the starting peak position has a blue shift with an increase in the excitation power because of the state filling as reported before.[9] At a low excitation power up to 7.5 μW, the peak position shows a quick blue shift first and then becomes

DOI: 10.1021/acsphotonics.6b00843
ACS Photonics 2017, 4, 369−377

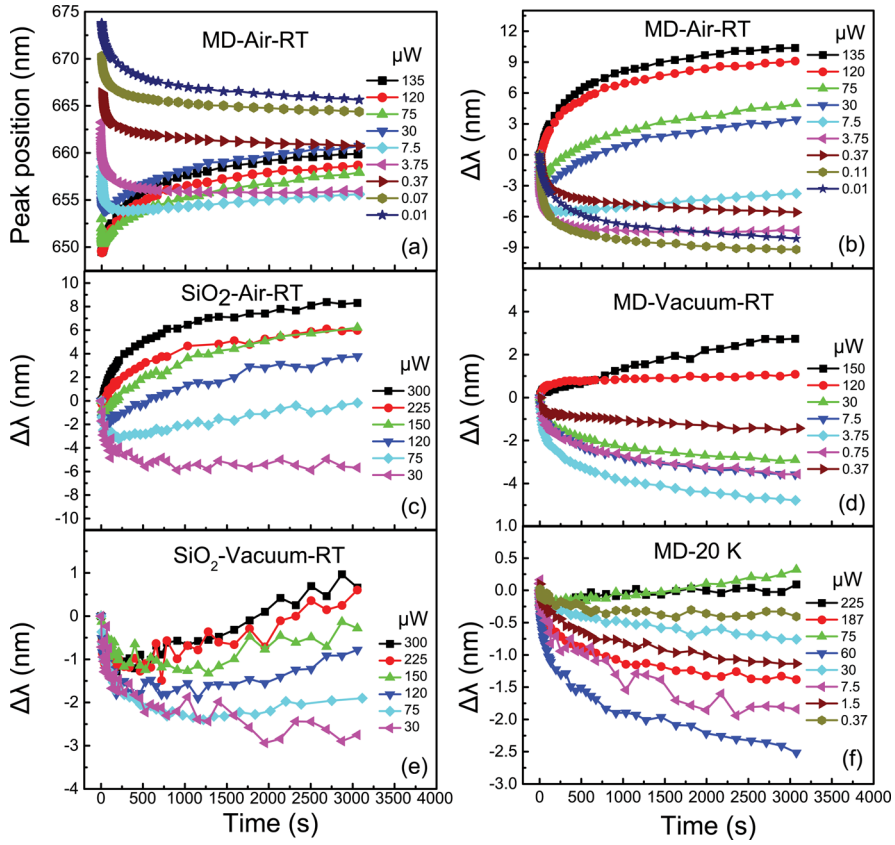

Figure 7. (a) PL peak positions as a function of time for QDs on MDs in air at RT. (b–f) Temporal evolution of PL peak position change ($\Delta\lambda$) with various excitation powers. The measurement conditions are marked in each panel.

stabilized as a function of exposure time. As the excitation power is further increased, the peak starts with a quick blue shift (less than 10 s) and then a slow red shift. In the end, when the excitation power is more than 120 μW, only a red shift can be observed within the time resolution in our measurement.

Because of the power-induced broadening, the line width of PL spectra increases generally with increasing excitation power without considering the time evolution, as shown in Figure 8a. In order to see the clear change of the PL spectra, we define $\Delta\lambda$ and Δfwhm as the difference between the first spectrum and the rest of the spectra of the central emission peak.[51] The $\Delta\lambda$ and Δfwhm as a function of excitation time with different pumping powers are shown in Figure 7b–f and Figure 8b–f, respectively. The PL blue shifts at a low excitation power exposed in air can be explained by photooxidation. During the illumination exposed in air, the surface of CIS QDs is oxidized when oxygen diffuses through the passivating layer of ZnS, which reduces the average sizes and broadens the size distribution of QDs.[22] The reduced sizes of QDs induce a blue shift because of the increased quantum confinement, which is similar to the results of CdSe/ZnS QDs.[4] The broadened size distribution induces a line width increase of the PL spectra, as shown in Figure 8b for the low excitation power cases of less than 30 μW.

One possible reason for the red shift could be the thermal expansion of QDs because of the increased sample temperature at a high excitation power. However, a surprising phenomenon is that the line width decreases with excitation power over 120 μW, as shown in Figure 8a and b. The red shift and the line width narrowing at high excitation power cannot be simply attributed to thermal expansion. Additionally, the line width narrowing with increasing pumping power could be due to the enhanced coupling between QDs and MDs, similar to a lasering effect. But it can also be excluded that enhanced spontaneous emission should not be necessarily coming along with a red shift. Therefore, we ascribe the red shift with line width narrowing to the agglomeration of QDs induced by high-intensity laser illumination. Because of the laser-induced OLA ligand damage, the average distances between QDs are reduced after the agglomeration. The reduced average distance enhances the Förster resonant energy transfer (FRET) between different QDs. The enhanced FRET from small QDs to large ones gives a red shift and a narrowed line width of the PL spectrum. Similar results on both the blue shift and red shift can be observed for the QDs on SiO_2/Si substrates, which are not as strong as the cases on the MDs, as shown in Figure 7c and Figure 8c. Although no line width narrowing can be observed of the QDs on SiO_2/Si substrates, the line width broadening slows down when the excitation power is more than 150 μW (green triangles in Figure 8c). This strengthens the claim that MDs accelerate the photooxidation with a high excitation power.

While under vacuum, both a blue shift and a red shift still can be observed with increasing excitation power on SiO_2/Si substrates and on MDs, as shown in Figure 7d and e. The photooxidation-induced blue shift can be ascribed to the absorption of oxygen on the QDs' surface under vacuum. The overall peak changes on both the blue shift and red shift are much less than those in air. In particular, a red shift is only about 3 nm with QDs on MDs under vacuum, compared with a 10 nm shift in air. This confirms that oxygen in the air is a key issue in photooxidation and photobleaching. No line width narrowing has been observed, as shown in Figure 8d and e. It

DOI: 10.1021/acsphotonics.6b00843
ACS Photonics 2017, 4, 369–377

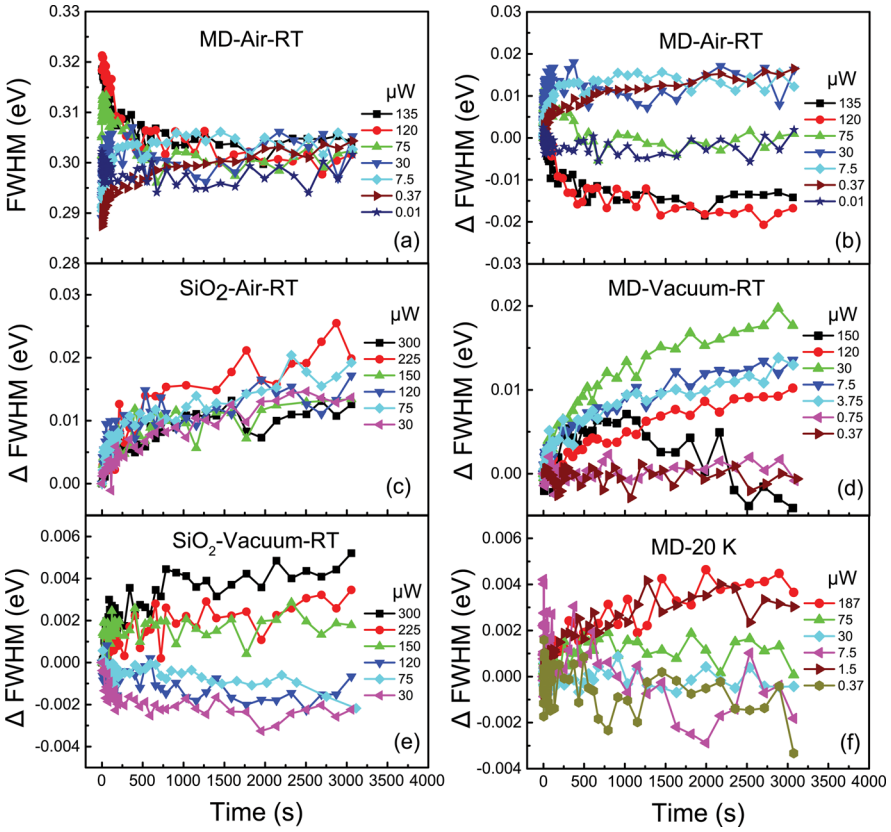

Figure 8. (a) PL line widths as a function of time for QDs on MDs in air at RT. (b–f) Temporal evolution of line width change (Δfwhm) with various excitation powers. The measurement conditions are marked in each panel.

should be emphasized that the PL peak shift and line width broadening can be negligible for QDs on MDs under vacuum with a small excitation power, for instance, 0.37 μW in Figures 7d and 8d. Figure 7f shows the PL peak shifts of QDs on the edge of MDs at 20 K as a function of time with different excitation powers, which are much less than those at RT (Figure 7b and d). As the excitation power increases up to 60 μW, the blue shifts become stronger, but get weaker with a further increase of excitation power. This can be explained in a similar way to the case under vacuum. The line widths do not change very much at 20 K (Figure 8f). In contrast to the case under vacuum at RT, the ligands of QDs are more easily damaged, resulting in faster photobleaching at 20 K. However, no strong red shift can be resolved even with a high excitation power, which shows that the QDs do not aggregate very much at low temperature.

To achieve a high fluorescence intensity, it is necessary to increase the pumping laser power. While due to the photooxidation and photobleaching, the PL intensity of CIS QDs drop-casted on SiO_2/Si substrates decreases because of the low collection efficiency within the irradiation time both in air and under vacuum. This can be solved by drop-casting QDs on MDs under vacuum, where the photodegradation can be avoided with a low excitation power because of the Purcell effect and the enhanced collection efficiency. Thus, a proper surface protection of CIS QDs on MDs could be used to obtain enhanced PL emission without photodegradation.

CONCLUSIONS

In summary, the temporal evolution of PL properties of CIS/ZnS QDs has been systematically investigated by drop-casting QDs on SiO_2/Si substrates and MDs in different atmospheric conditions. In air, strong photodegradation has been observed because of the photooxidation and photobleaching accompanying a PL peak blue shift and line width broadening at low excitation power. With a further increase in the excitation power, the PL spectra have shown a red shift and narrowing line width. This is due to the fact that the photoinduced ligand damage induces the agglomeration of QDs, which enhances FRET between different QDs. The enhanced FRET gives a red shift and a reduced line width. All these photobleaching effects are reduced under vacuum, which shows that oxygen plays an important role in the optically induced PL decay. When the QDs are drop-casted on MDs, the pumping laser and emitted photon energy couple with the cavity modes of the MDs. When the pumping laser couples with leaky modes in the MDs, the excitation efficiency is greatly enhanced, which accelerates photobleaching. When the QDs couple with cavity modes, however, the extraction efficiency is greatly improved because of the Purcell effect, resulting in a PL enhancement by 20 times at RT and by 35 times at 20 K. By taking advantages of enhanced PL extraction efficiency, photobleaching can be avoided with a small excitation power but with a relatively high PL intensity. Since photodegradation has been one of the major obstacles for using colloidal QDs in many applications, the highly efficient PL emission without photodegradation is very promising for utilizing CIS QDs as highly efficient photon emitters at RT. This paves a new way for CIS QDs to implement single-photon emission at RT for quantum information processing, instead of InAs QDs working at cryogenic temperature.[49,52]

DOI: 10.1021/acsphotonics.6b00843
ACS Photonics 2017, 4, 369–377

METHODS

The CIS/ZnS QDs were synthesized by thermolysis with a mixture solution of copper(I) acetate, indium acetate, and oleylamine as ligands in a high boiling point solvent at 240 °C. The details of the synthesis process can be found in our previous reports.[6,53] The CIS/ZnS core/shell QDs have diameters of about 2−5 nm and exhibit a tunable PL emission wavelength range from 500 to 900 nm.[19] The CIS QD powder was dissolved in toluene assisted by ultrasonic vibration, then drop-casted on a SiO_2/Si substrate or a silica MD.[42] After the toluene was evaporated, the close-packed QD solids were formed.[54] Steady-state PL spectra were measured by a conventional confocal micro-PL system, as shown in Figure 1. The CIS QD samples were placed in a coldfinger cryostat with an optical window for PL measurement, with which the sample temperature can be tuned from 20 K to RT. An excitation laser with a wavelength of 532 nm was focused on the samples by using a large numerical aperture objective with a spot size around 1−2 μm in diameter. The objective is mounted on a two-dimensional PZT-controlled stage for spatial mapping. The excitation laser power was measured after the objective above the samples. The fluorescence from CIS/ZnS QDs was collected by the same objective and then dispersed through a 0.55 m spectrometer. The PL spectrum was measured by a charge-coupled device camera cooled with liquid nitrogen. The inset of Figure 1 shows a scanning electron microscope (SEM) image of the cross section of a silica MD. The diameter of the MD is around 150 μm, which is marked in Figure 1. The WGMs are confined at the edge of the MD, which induces high quality factors. The quality factors in the wavelength range of QDs are about 10^6, by a transmission measurement using a tunable semiconductor laser around 635 nm.[42]

A 2D simulation has been performed to calculate the mode distribution for a microdisk with a radius of 75 μm using the finite-difference time-domain method. A refractive index of 1.456 was used, which should be suitable for the emission wavelength range of CIS QDs, from 600 to 800 nm. A magnetic dipole (corresponding to the TE mode) at 563 THz with a pulse width of 3.5 fs was put 74.2 μm away from the center. The simulation region is a square with a side length of 160 μm, and the mesh is 25 nm in both the x and y directions. A mode position at 669.75 nm has been selected to calculate the electromagnetic field distribution, which is close to the peak position of PL emission from QDs, as shown in Figure 2d.

AUTHOR INFORMATION

Corresponding Author

*E-mail (X. Xu): xlxu@iphy.ac.cn.

ORCID

Haizheng Zhong: 0000-0002-2662-7472

Kuijuan Jin: 0000-0002-0047-4375

Xiulai Xu: 0000-0001-8231-406X

Notes

The authors declare no competing financial interest.

ACKNOWLEDGMENTS

This work was supported by the National Basic Research Program of China under Grant Nos. 2013CB328706 and 2014CB921003; the National Natural Science Foundation of China under Grant Nos. 91436101, 61675228, and 61275060; and the Strategic Priority Research Program of the Chinese Academy of Sciences under Grant No. XDB07030200.

REFERENCES

(1) Klimov, V. I.; McBranch, D. W. Femtosecond 1*P*-to- 1*S* electron relaxation in strongly confined semiconductor nanocrystals. *Phys. Rev. Lett.* **1998**, *80*, 4028−4031.

(2) Klimov, V. I.; Mikhailovsky, A. A.; McBranch, D. W.; Leatherdale, C. A.; Bawendi, M. G. Quantization of multiparticle Auger rates in semiconductor quantum dots. *Science* **2000**, *287*, 1011−1013.

(3) Guo, W.; Li, J.; Wang, Y.; Peng, X. Luminescent CdSe/CdS core/shell nanocrystals in dendron boxes: Superior chemical, photochemical and thermal stability. *J. Am. Chem. Soc.* **2003**, *125*, 3901−3909.

(4) van Sark, W.; Frederix, P.; Van den Heuvel, D.; Gerritsen, H.; Bol, A.; van Lingen, J.; Donega, C.; Meijerink, A. Photooxidation and photobleaching of single CdSe/ZnS quantum dots probed by room-temperature time-resolved spectroscopy. *J. Phys. Chem. B* **2001**, *105*, 8281−8284.

(5) Nazzal, A.; Wang, X.; Qu, L.; Yu, W.; Wang, Y.; Peng, X.; Xiao, M. Environmental effects on photoluminescence of highly luminescent CdSe and CdSe/ZnS core/shell nanocrystals in polymer thin films. *J. Phys. Chem. B* **2004**, *108*, 5507−5515.

(6) Chen, B.; Zhong, H.; Zhang, W.; Tan, Z.; Li, Y.; Yu, C.; Zhai, T.; Bando, Y.; Yang, S.; Zou, B. Highly emissive and color-tunable $CuInS_2$-based colloidal semiconductor nanocrystals: Off-stoichiometry effects and improved electroluminescence performance. *Adv. Funct. Mater.* **2012**, *22*, 2081−2088.

(7) Li, Q.; Zhai, L.; Zou, C.; Huang, X.; Zhang, L.; Yang, Y.; Chen, X.; Huang, S. Wurtzite $CuInS_2$ and $CuInxGa_{1-x}S_2$ nanoribbons: Synthesis, optical and photoelectrical properties. *Nanoscale* **2013**, *5*, 1638−1648.

(8) Akdas, T.; Walter, J.; Segets, D.; Distaso, M.; Winter, B.; Birajdar, B.; Spiecker, E.; Peukert, W. Investigation of the size-property relationship in $CuInS_2$ quantum dots. *Nanoscale* **2015**, *7*, 18105−18118.

(9) Sun, Y.; Qian, C.; Peng, K.; Bai, Z.; Tang, J.; Zhao, Y.; Wu, S.; Ali, H.; Song, F.; Zhong, H.; et al. Recombination processes in $CuInS_2$/ZnS nanocrystals during steady-state photoluminescence. *Appl. Phys. Lett.* **2016**, *108*, 041106.

(10) Shabaev, A.; Mehl, M. J.; Efros, A. L. Energy band structure of $CuInS_2$ and optical spectra of $CuInS_2$ nanocrystals. *Phys. Rev. B: Condens. Matter Mater. Phys.* **2015**, *92*, 035431.

(11) Pan, Z.; Mora-Sero, I.; Shen, Q.; Zhang, H.; Li, Y.; Zhao, K.; Wang, J.; Zhong, X.; Bisquert, J. High-efficiency green quantum dot solar cells. *J. Am. Chem. Soc.* **2014**, *136*, 9203−9210.

(12) Zhao, K.; Pan, Z.; Mora-Sero, I.; Canovas, E.; Wang, H.; Song, Y.; Gong, X.; Wang, J.; Bonn, M.; Bisquert, J.; et al. Boosting power conversion efficiencies of quantum-dot-sensitized solar cells beyond 8% by recombination control. *J. Am. Chem. Soc.* **2015**, *137*, 5602−5609.

(13) Knowles, K. E.; Hartstein, K. H.; Kilburn, T. B.; Marchioro, A.; Nelson, H. D.; Whitham, P. J.; Gamelin, D. R. Luminescent colloidal semiconductor nanocrystals containing copper: Synthesis, photophysics, and applications. *Chem. Rev.* **2016**, *116*, 10820.

(14) Li, L.; Pandey, A.; Werder, D. J.; Khanal, B. P.; Pietryga, J. M.; Klimov, V. I. Efficient synthesis of highly luminescent copper indium sulfide-based core/shell nanocrystals with surprisingly long-lived emission. *J. Am. Chem. Soc.* **2011**, *133*, 1176−1179.

(15) Leach, A. D. P.; Macdonald, J. E. Optoelectronic properties of $CuInS_2$ nanocrystals and their origin. *J. Phys. Chem. Lett.* **2016**, *7*, 572−583.

(16) Whitham, P. J.; Marchioro, A.; Knowles, K. E.; Kilburn, T. B.; Reid, P. J.; Gamelin, D. R. Single-particle photoluminescence spectra, blinking, and delayed luminescence of colloidal $CuInS_2$ nanocrystals. *J. Phys. Chem. C* **2016**, *120*, 17136−17142.

(17) Berends, A. C.; Rabouw, F. T.; Spoor, F. C. M.; Bladt, E.; Grozema, F. C.; Houtepen, A. J.; Siebbeles, L. D. A.; de Mello Donegá, C. Radiative and nonradiative recombination in $CuInS_2$ nanocrystals

DOI: 10.1021/acsphotonics.6b00843
ACS Photonics 2017, 4, 369−377

and $CuInS_2$-based core/shell nanocrystals. *J. Phys. Chem. Lett.* **2016**, *7*, 3503−3509.
(18) Knowles, K. E.; Nelson, H. D.; Kilburn, T. B.; Gamelin, D. R. Singlet-triplet splittings in the luminescent excited states of colloidal Cu^+:CdSe, Cu^+:InP, and $CuInS_2$ nanocrystals: charge-transfer configurations and self-trapped excitons. *J. Am. Chem. Soc.* **2015**, *137*, 13138−13147.
(19) Zhong, H.; Bai, Z.; Zou, B. Tuning the luminescence properties of colloidal I-III-VI semiconductor nanocrystals for optoelectronics and biotechnology applications. *J. Phys. Chem. Lett.* **2012**, *3*, 3167−3175.
(20) Shi, A.; Wang, X.; Meng, X.; Liu, X.; Li, H.; Zhao, J. Temperature-dependent photoluminescence of $CuInS_2$ quantum dots. *J. Lumin.* **2012**, *132*, 1819−1823.
(21) Omata, T.; Nose, K.; Kurimoto, K.; Kita, M. Electronic transition responsible for size-dependent photoluminescence of colloidal $CuInS_2$ quantum dots. *J. Mater. Chem. C* **2014**, *2*, 6867−6872.
(22) Manner, V. W.; Koposov, A. Y.; Szymanski, P.; Klimov, V. I.; Sykora, M. Role of solvent-oxygen ion pairs in photooxidation of CdSe nanocrystal quantum dots. *ACS Nano* **2012**, *6*, 2371−2377.
(23) Zhang, A.; Dong, C.; Li, L.; Yin, J.; Liu, H.; Huang, X.; Ren, J. Non-blinking (Zn)CuInS/ZnS quantum dots prepared by in situ interfacial alloying approach. *Sci. Rep.* **2015**, *5*, 15227.
(24) Vahala, K. Optical microcavities. *Nature* **2003**, *424*, 839−846.
(25) Tang, J.; Geng, W.; Xu, X. Quantum interference induced photon blockade in a coupled single quantum dot-cavity system. *Sci. Rep.* **2015**, *5*, 9252.
(26) Zhang, Y.; Komarala, V. K.; Rodriguez, C.; Xiao, M. Controlling fluorescence intermittency of a single colloidal CdSe/ZnS quantum dot in a half cavity. *Phys. Rev. B: Condens. Matter Mater. Phys.* **2008**, *78*, 241301.
(27) Yang, J.; Heo, J.; Zhu, T.; Xu, J.; Topolancik, J.; Vollmer, F.; Ilic, R.; Bhattacharya, P. Enhanced photoluminescence from embedded PbSe colloidal quantum dots in silicon-based random photonic crystal microcavities. *Appl. Phys. Lett.* **2008**, *92*, 261110.
(28) Kahl, M.; Thomay, T.; Kohnle, V.; Beha, K.; Merlein, J.; Hagner, M.; Halm, A.; Ziegler, J.; Nann, T.; Fedutik, Y.; et al. Colloidal quantum dots in all-dielectric high-Q pillar microcavities. *Nano Lett.* **2007**, *7*, 2897−2900.
(29) Gupta, S.; Waks, E. Spontaneous emission enhancement and saturable absorption of colloidal quantum dots coupled to photonic crystal cavity. *Opt. Express* **2013**, *21*, 29612−29619.
(30) Pattantyus-Abraham, A. G.; Qiao, H.; Shan, J.; Abel, K. A.; Wang, T.-S.; van Veggel, F. C. J. M.; Young, J. F. Site-selective optical coupling of PbSe nanocrystals to Si-based photonic crystal microcavities. *Nano Lett.* **2009**, *9*, 2849−2854.
(31) Martiradonna, L.; Carbone, L.; Tandaechanurat, A.; Kitamura, M.; Iwamoto, S.; Manna, L.; De Vittorio, M.; Cingolani, R.; Arakawa, Y. Two-dimensional photonic crystal resist membrane nanocavity embedding colloidal dot-in-a-rod nanocrystals. *Nano Lett.* **2008**, *8*, 260−264.
(32) Foell, C. A.; Schelew, E.; Qiao, H.; Abel, K. A.; Hughes, S.; van Veggel, F. C. J. M.; Young, J. F. Saturation behaviour of colloidal PbSe quantum dot exciton emission coupled into silicon photonic circuits. *Opt. Express* **2012**, *20*, 10453−10469.
(33) Ganesh, N.; Zhang, W.; Mathias, P.; Chow, E.; Soares, J.; Malyarchuk, V.; Smith, A.; Cunningham, B. Enhanced fluorescence emission from quantum dots on a photonic crystal surface. *Nat. Nanotechnol.* **2007**, *2*, 515−520.
(34) Rodarte, A. L.; Gray, C.; Hirst, L. S.; Ghosh, S. Spectral and polarization modulation of quantum dot emission in a one-dimensional liquid crystal photonic cavity. *Phys. Rev. B: Condens. Matter Mater. Phys.* **2012**, *85*, 035430.
(35) Rakovich, A.; Albella, P.; Maier, S. A. Plasmonic control of radiative properties of semiconductor quantum dots coupled to plasmonic ring cavities. *ACS Nano* **2015**, *9*, 2648−2658.
(36) Hoang, T. B.; Akselrod, G. M.; Mikkelsen, M. H. Ultrafast room-temperature single photon emission from quantum dots coupled to plasmonic nanocavities. *Nano Lett.* **2016**, *16*, 270−275.
(37) Yoshie, T.; Scherer, A.; Hendrickson, J.; Khitrova, G.; Gibbs, H.; Rupper, G.; Ell, C.; Shchekin, O.; Deppe, D. Vacuum Rabi splitting with a single quantum dot in a photonic crystal nanocavity. *Nature* **2004**, *432*, 200−203.
(38) Reithmaier, J.; Sek, G.; Loffler, A.; Hofmann, C.; Kuhn, S.; Reitzenstein, S.; Keldysh, L.; Kulakovskii, V.; Reinecke, T.; Forchel, A. Strong coupling in a single quantum dot-semiconductor microcavity system. *Nature* **2004**, *432*, 197−200.
(39) Hennessy, K.; Badolato, A.; Winger, M.; Gerace, D.; Atature, M.; Gulde, S.; Falt, S.; Hu, E.; Imamoglu, A. Quantum nature of a strongly coupled single quantum dot-cavity system. *Nature* **2007**, *445*, 896−899.
(40) Srinivasan, K.; Painter, O. Linear and nonlinear optical spectroscopy of a strongly coupled microdisk-quantum dot system. *Nature* **2007**, *450*, 862−865.
(41) Brossard, F. S. F.; Xu, X. L.; Williams, D. A.; Hadjipanayi, M.; Hugues, M.; Hopkinson, M.; Wang, X.; Taylor, R. A. Strongly coupled single quantum dot in a photonic crystal waveguide cavity. *Appl. Phys. Lett.* **2010**, *97*, 111101.
(42) Bo, F.; Huang, S.; Ozdemir, S.; Zhang, G.; Xu, J.; Yang, L. Inverted-wedge silica resonators for controlled and stable coupling. *Opt. Lett.* **2014**, *39*, 1841−1844.
(43) Xie, W.; Zhu, Y.; Aubert, T.; Hens, Z.; Brainis, E.; Thourhout, D. V. Fabrication and characterization of on-chip silicon nitride microdisk integrated with colloidal quantum dots. *Opt. Express* **2016**, *24*, A114−A122.
(44) Sykora, M.; Koposov, A.; McGuire, J.; Schulze, R.; Tretiak, O.; Pietryga, J.; Klimov, V. Effect of air exposure on surface properties, electronic structure, and carrier relaxation in PbSe nanocrystals. *ACS Nano* **2010**, *4*, 2021.
(45) Giebink, N.; Wiederrecht, G.; Wasielewski, M. Strong exciton-photon coupling with colloidal quantum dots in a high-Q bilayer microcavity. *Appl. Phys. Lett.* **2011**, *98*, 081103.
(46) Michler, P.; Imamoglu, A.; Mason, M. D.; Carson, P. J.; Strouse, G. F.; Buratto, S. K. Quantum correlation among photons from a single quantum dot at room temperature. *Nature* **2000**, *406*, 968−970.
(47) Brokmann, X.; Messin, G.; Desbiolles, P.; Giacobino, E.; Dahan, M.; Hermier, J. Colloidal CdSe/ZnS quantum dots as single-photon sources. *New J. Phys.* **2004**, *6*, 99.
(48) Wissert, M. D.; Rudat, B.; Lemmer, U.; Eisler, H.-J. Quantum dots as single-photon sources: Antibunching via two-photon excitation. *Phys. Rev. B: Condens. Matter Mater. Phys.* **2011**, *83*, 113304.
(49) Xu, X.; Williams, D.; Cleaver, J. Electrically pumped single-photon sources in lateral p-i-n junctions. *Appl. Phys. Lett.* **2004**, *85*, 3238.
(50) Wang, X.; Zhang, J.; Nazzal, A.; Xiao, M. Photo-oxidation-enhanced coupling in densely packed CdSe quantum-dot films. *Appl. Phys. Lett.* **2003**, *83*, 162.
(51) Pankiewicz, C.; de Assis, P.; Cabral, P.; Chaves, C.; de Araujo, E.; Paniago, R.; Guimaraes, P. Characterization of the dynamics of photoluminescence degradation in aqueous CdTe/CdS core-shell quantum dots. *J. Fluoresc.* **2015**, *25*, 1389−1395.
(52) Xu, X. L.; Toft, I.; Phillips, R. T.; Mar, J.; Hammura, K.; Williams, D. A. Plug and play" single-photon sources. *Appl. Phys. Lett.* **2007**, *90*, 061103.
(53) Bai, Z.; Ji, W.; Han, D.; Chen, L.; Chen, B.; Shen, H.; Zou, B.; Zhong, H. Hydroxyl-terminated $CuInS_2$ based quantum dots: Toward efficient and bright light emitting diodes. *Chem. Mater.* **2016**, *28*, 1085−1091.
(54) Pan, S. S.; Li, F. D.; Liu, Q. W.; Xu, S. C.; Luo, Y. Y.; Li, G. H. Strong localization induced anomalous temperature dependence exciton emission above 300K from SnO_2 quantum dots. *J. Appl. Phys.* **2015**, *117*, 173101.

DOI: 10.1021/acsphotonics.6b00843
ACS Photonics 2017, 4, 369−377